Pré-Publicações do Departamento de Matemática
Universidade de Coimbra
Preprint Number 09–02

NUMERICAL APPROXIMATION OF A DIFFUSIVE HYPERBOLIC EQUATION

A. ARAÚJO, C. NEVES AND E. SOUSA

Abstract: In this work numerical methods for one-dimensional diffusion problems are discussed. The differential equation considered, takes into account the variation of the relaxation time of the mass flux and the existence of a potential field. Consequently, according to which values of the relaxation parameter or the potential field we assume, the equation can have properties similar to a hyperbolic equation or to a parabolic equation. The numerical schemes consist of using an inverse Laplace transform algorithm to remove the time-dependent terms in the governing equation and boundary conditions. For the spatial discretisation, three different approaches are discussed and we show their advantages and disadvantages according to which values of the potential field and relaxation time parameters we choose.

Keywords: Diffusion, hyperbolic equation, inverse Laplace transform, error analysis.
AMS Subject Classification (2000): 35Q80, 65M12, 65D30.

1. Introduction

The classical way to treat the diffusion problem of a Brownian particle is to start with the well known Fick's law for the mass flux

$$J(x,t) = -D\frac{\partial c}{\partial x}(x,t),$$

where c is the mass concentration of the Brownian particle and D is the diffusion coefficient. If we combine this equation with the mass conservation law (or continuity equation)

$$\frac{\partial c}{\partial t}(x,t) + \frac{\partial J}{\partial x}(x,t) = 0, \tag{1}$$

the dynamics of a Brownian particle is described by the diffusion equation

$$\frac{\partial c}{\partial t}(x,t) = D\frac{\partial^2 c}{\partial x^2}(x,t). \tag{2}$$

When a uniform force field such as gravitation exists, a uniform flow is produced with the terminal velocity determined by the balance of the driving

Received January 9, 2009.

force and the frictional force from the surrounding fluid acting on the particle [11]. Therefore, the flow is given by

$$J(x,t) = -D\frac{\partial c}{\partial x}(x,t) - P(x)c(x,t), \tag{3}$$

where

$$P(x) = \frac{1}{m\gamma}\frac{dV}{dx}(x),$$

V is the potential field, m is the particle mass and γ the friction constant. The diffusion constant can also be written as

$$D = \kappa_B \frac{T}{m\gamma},$$

where κ_B is the Boltzmann constant and T is the temperature of the fluid.

As it was been pointed out by several authors, equation (2) presents an unphysical property: if a sudden change in the concentration is made at a point, it will be felt instantly everywhere. This property, known as infinite speed of propagation, is not present in mass diffusion phenomena and therefore we have the violation of the principle of causality. This turns out to be a problem, specially if we are interested in the transient problem in a short period of time, or for low temperature [13]. In order to describe the mass diffusion with a finite speed of propagation, we must consider the so-called non-Fickian diffusion equations. Das [6, 7] has derived a non-Fickian diffusion equation in the presence of a potential field from the Kramer's equation. This equation is a hyperbolic equation, although the corresponding Fickian equation is a parabolic equation.

To accommodate the finite propagation speed, the generalized Fick's law can be written as [7]

$$\theta\frac{\partial J}{\partial t}(x,t) + J(x,t) = -D\frac{\partial c}{\partial x}(x,t) - P(x)c(x,t), \tag{4}$$

where $\theta = \frac{1}{\gamma} \in]0,1]$ is the parameter that measures the propagation speed of the mass wave and can be regarded as the relaxation time of the mass flux. In fact, if we assume that the mass flux at point x and time t results from the concentration gradient at x but at some passed time instead of (3), we must consider

$$J(x,t+\theta) = -D\frac{\partial c}{\partial x}(x,t) - P(x)c(x,t),$$

where θ is a small parameter. Considering a first order approximation to the flux we can obtain (4). Integrating the first order differential equation (4), we obtain the generalization of the Cattaneo's law for the flux [10]

$$J(x,t) = -\frac{1}{\theta}\int_0^t \mathrm{e}^{-\frac{t-s}{\theta}} \left(D\frac{\partial c}{\partial x}(x,s) + P(x)c(x,s) \right) ds.$$

Elimination of the mass flux J between equations (1) and (4) leads to the equation

$$\frac{\partial c}{\partial t}(x,t) = \frac{1}{\theta}\int_0^t \mathrm{e}^{-\frac{t-s}{\theta}} \left(D\frac{\partial^2 c}{\partial x^2}(x,s) + \frac{\partial}{\partial x}\left(P(x)c(x,s)\right) \right) ds. \tag{5}$$

If we impose some regularity conditions on the initial condition, it may be proven that (5) is equivalent to the hyperbolic telegraph equation

$$\frac{\partial c}{\partial t} + \theta\frac{\partial^2 c}{\partial t^2} = \frac{\partial}{\partial x}(Pc) + D\frac{\partial^2 c}{\partial x^2}, \quad x \in \left]0,\infty\right[, t > 0. \tag{6}$$

For our problem we consider the initial conditions given by

$$c(x,0) = 0, \qquad x \in [0,\infty[, \tag{7}$$
$$\theta\frac{\partial c}{\partial t}(x,0) = 0, \qquad x \in [0,\infty[\tag{8}$$

and the boundary conditions

$$c(0,t) = f(t), \qquad t > 0, \tag{9}$$
$$c(\infty,t) = 0, \qquad t > 0. \tag{10}$$

Equation (6) is a more general equation than the ones presented in works, such as [3, 4, 9, 13, 15]. In order to study problems of hyperbolic type and parabolic type, we consider $\theta \in [0,1]$, since the parameter θ is directly related with the parabolic or hyperbolic behavior of equation (6). For $\theta \neq 0$, this problem transmits waves with finite velocity [8]. Note that, for $\theta = 0$, equation (6) is the classical parabolic advection-diffusion equation. In this work, we present numerical methods that can be considered for both cases, the parabolic case and the hyperbolic case being the latter usually more difficult to handle.

2. The numerical schemes

In this section we describe the numerical methods applied to solve the problem (6)–(10). Our approach can be separated in three steps. First, we apply the Laplace transform to (6)–(10) in order to remove the time dependent terms and we obtain an ordinary differential equation in x that also depends on the Laplace transform parameter s. Secondly, we solve the ordinary differential equation obtained using three different space discretisations: the first one is a finite volume discretisation suggested in [2], the second one is a piecewise linearized method suggested in [14] and the third one is a finite difference scheme proposed by us, which considers the central difference approximations for the first and second derivatives with the purpose of comparing the previous two methods with more well known discretisations and henceforth to highlight their advantages and disadvantages. Lastly, using a numerical inverse Laplace transform algorithm, suggested in [1], we obtain the final approximated solution.

Let us start to describe the Laplace transform technique, which removes the t-dependent terms.

The Laplace transform $\widetilde{c}$ of the mass concentration c is defined by

$$\widetilde{c}\,(x,s) = \int_0^\infty \mathrm{e}^{-st} c\,(x,t)\,dt.$$

We obtain the ordinary differential equation

$$\frac{d^2\widetilde{c}}{dx^2} - \lambda_s^2 \widetilde{c} + \frac{d}{dx}\left(\frac{P}{D}\widetilde{c}\right) = 0 \qquad (11)$$

where $\lambda_s = \left(\left(\theta s^2 + s\right)/D\right)^{1/2}$ and s is a complex variable.

If P is a constant, then we easily obtain the exact solution of equation (11)

$$\widetilde{c}\,(x,s) = A\mathrm{e}^{\nu_s^+ x} + B\mathrm{e}^{\nu_s^- x}, \qquad (12)$$

for $\nu_s^\pm = -\frac{P}{2D} \pm \sqrt{R_s}$, with $R_s = \left(\frac{P}{2D}\right)^2 + \lambda_s^2$, and A, B are constants to be determined. From the boundary conditions (9)–(10) we get

$$\widetilde{c}\,(0,s) = \widetilde{f}(s) \;\text{ and }\; \widetilde{c}\,(\infty,s) = 0. \qquad (13)$$

The substitution of these conditions in (12) implies that

$$\widetilde{c}\,(x,s) = \widetilde{f}(s)\mathrm{e}^{\nu_s^- x}.$$

For $f(t) = c_0$ we have

$$\widetilde{c}\,(x,s) = c_0 \frac{1}{s} \mathrm{e}^{\nu_s^- x}. \tag{14}$$

In the following sections, we present the space discretisations and we describe the algorithm used to perform the Laplace inversion. If P is constant we do not need to do a space discretisation and therefore we can directly apply the inverse Laplace transform algorithm. For non-constant P the spatial discretisation is mandatory.

2.1. Space discretisation. In this section we consider three different ways of discretising the ordinary differential equation (11). The three methods can be written in the form of a matrix iteration. Assume we have a space discretisation $x_i = i\Delta x,\ i = 0, \ldots, N$. Let $\widetilde{C}_i(s),\ i = 0, \ldots, N$ represent the approximation of $\widetilde{c}\,(x_i, s)$ in the Laplace transform domain. The outflow boundary is such that $\widetilde{C}_N(s) = 0$, for all s and N sufficiently large, which is according to the physical boundary condition (13). After the spatial discretisation we obtain the linear system

$$K\,(s)\,\widetilde{\mathbf{C}}\,(s) = \widetilde{b}\,(s)\,, \tag{15}$$

where $K(s) = [K_{i,j}(s)]$ is a band matrix of size $N-1 \times N-1$ with bandwidth three, $\widetilde{\mathbf{C}}\,(s) = [\widetilde{C}_1\,(s)\,, \ldots, \widetilde{C}_{N-1}\,(s)]^T$ and $\widetilde{b}\,(s)$ contains boundary conditions, being represented by

$$\widetilde{b}\,(s) = \begin{bmatrix} -K_{1,0}(s)\widetilde{C}_0(s) \\ 0 \\ \vdots \\ 0 \\ -K_{N-1,N}(s)\widetilde{C}_N(s) \end{bmatrix}.$$

In what follows, we present the space discretisations by giving the entries of the matrix K. As we have seen above the matrix K and the discretisation points depend on s. In the next two sections and in the sake of clarity we omit the parameter s denoting $K_{i,j}(s)$ and $\widetilde{C}_i(s)$ by $K_{i,j}$ and $\widetilde{C}_i$ respectively.

2.1.1. *Finite volumes.* The ordinary differential equation (11) is discretised using a finite volume formulation by integrating the ordinary differential equation in the i-th control volume $[x_i - \Delta x/2, x_i + \Delta x/2]$,

$$\int_{x_i-\Delta x/2}^{x_i+\Delta x/2} \left[\frac{d^2\widetilde{C}}{dx^2} - \lambda_s^2 \widetilde{C} + \frac{d}{dx}\left(\frac{P}{D}\widetilde{C}\right)\right] dx$$

where $\widetilde{C}(x,s)$ is an approximation of $\widetilde{c}(x,s)$. As suggested in [2], for $x \in [x_i, x_{i+1}]$, $i = 0, \dots, N-1$, we approximate $\widetilde{c}\,(x,s)$ by the following combination of hyperbolic functions,

$$\widetilde{C}\,(x,s) = \frac{\sinh\left(\lambda_s\left(x_{i+1}-x\right)\right)}{\sinh\left(\lambda_s \Delta x\right)}\widetilde{C}_i + \frac{\sinh\left(\lambda_s\left(x-x_i\right)\right)}{\sinh\left(\lambda_s \Delta x\right)}\widetilde{C}_{i+1}.$$

The evaluation of the integral produces the following discretised equations

$$K_{i,i-1}\widetilde{C}_{i-1} + K_{i,i}\widetilde{C}_i + K_{i,i+1}\widetilde{C}_{i+1} = 0, \qquad i = 1, \dots, N-1, \tag{16}$$

for

$$\begin{aligned} K_{i,i-1} &= 1 - P_{i-1/2}\frac{\sinh\left(\lambda_s \Delta x/2\right)}{D\lambda_s} \\ K_{i,i} &= -2\cosh\left(\lambda_s\Delta x\right) + \left(P_{i+1/2} - P_{i-1/2}\right)\frac{\sinh\left(\lambda_s \Delta x/2\right)}{D\lambda_s} \\ K_{i,i+1} &= 1 - P_{i+1/2}\frac{\sinh\left(\lambda_s \Delta x/2\right)}{D\lambda_s}, \end{aligned}$$

where $P_{i\pm 1/2} = P\left(x_i \pm \Delta x/2\right)$. Therefore, equation (16) can be written in the matrix form (15) with matrix K defined by the entries given above.

2.1.2. *Piecewise linearized method.* Now we describe the space discretisation suggested in [14]. We can write equation (11) in the form

$$\frac{d^2\widetilde{c}}{dx^2} + \frac{P}{D}\frac{d\widetilde{c}}{dx} + \left(\frac{P'}{D} - \lambda_s^2\right)\widetilde{c} = 0, \tag{17}$$

P' represents the x derivative of P. In each interval $[x_{i-1}, x_{i+1}]$ the equation can be approximated by

$$\frac{d^2\widetilde{C}}{dx^2} + \frac{P_i}{D}\frac{d\widetilde{C}}{dx} + \left(\frac{P_i'}{D} - \lambda_s^2\right)\widetilde{C} = 0, \tag{18}$$

where $\widetilde{C}(x,s)$ represents an approximation of $\widetilde{c}(x,s)$, $P_i = P(x_i)$ and $P_i' = P'(x_i)$. This equation is obtained from (17) by freezing the coefficients at the mid-point of the considered interval. The solution of (18) in $[x_{i-1}, x_{i+1}]$ is

$$\widetilde{C}(x,s) = A_i \mathrm{e}^{\nu_{s,i}^{+}(x-x_i)} + B_i \mathrm{e}^{\nu_{s,i}^{-}(x-x_i)}. \tag{19}$$

The values A_i and B_i can be determined from (19) as

$$A_i = \frac{\widetilde{C}_{i-1} - \widetilde{C}_i \mathrm{e}^{-\nu_{s,i}^- \Delta x}}{\mathrm{e}^{-\nu_{s,i}^+ \Delta x} - \mathrm{e}^{-\nu_{s,i}^- \Delta x}} = \frac{\widetilde{C}_{i+1} - \widetilde{C}_i \mathrm{e}^{\nu_{s,i}^- \Delta x}}{\mathrm{e}^{\nu_{s,i}^+ \Delta x} - \mathrm{e}^{\nu_{s,i}^- \Delta x}}, \tag{20}$$

$$B_i = \widetilde{C}_i - A_i, \tag{21}$$

where $\nu_{s,i}^{\pm} = -\frac{P_i}{2D} \pm \sqrt{R_{s,i}}$, assuming $R_{s,i} = \left(\frac{P_i}{2D}\right)^2 + (\lambda_\theta^2 - P_i') > 0$. From (20)–(21) we obtain the following three-point finite difference equation

$$K_{i,i-1}\widetilde{C}_{i-1} + K_{i,i}\widetilde{C}_i + K_{i,i+1}\widetilde{C}_{i+1} = 0, \qquad i = 1, \ldots, N-1$$

where

$$\begin{aligned} K_{i,i-1} &= \mathrm{e}^{(\nu_{s,i}^+ + \nu_{s,i}^-)\Delta x}, \\ K_{i,i} &= -\mathrm{e}^{\nu_{s,i}^+ \Delta x} - \mathrm{e}^{\nu_{s,i}^- \Delta x}, \\ K_{i,i+1} &= 1. \end{aligned}$$

We expect this method to be less oscillatory than the one of the previous section as mentioned in [14].

2.1.3. *Finite differences.* For the finite differences discretisation we consider central differences to approximate the first derivative and the second derivative of equation (11),

$$\frac{\widetilde{C}_{i-1} - 2\widetilde{C}_i + \widetilde{C}_{i+1}}{\Delta x^2} - \lambda_s^2 \widetilde{C}_i + \frac{P_i}{D}\frac{\widetilde{C}_{i+1} - \widetilde{C}_{i-1}}{2\Delta x} = 0, \qquad i = 1, \ldots, N-1.$$

Therefore the matrix K has entries of the form

$$\begin{aligned} K_{i,i-1} &= \frac{1}{\Delta x^2} - \lambda_s^2 - \frac{P_i}{2D\Delta x}, \\ K_{i,i} &= -\frac{1}{\Delta x^2} - \lambda_s^2, \\ K_{i,i+1} &= \frac{1}{\Delta x^2} - \lambda_s^2 + \frac{P_i}{2D\Delta x}. \end{aligned}$$

2.2. Laplace transform inversion. The next step is to determine an approximated solution $C(x_i, t)$ from $\widetilde{C}(x_i, s)$ by using a Laplace inversion numerical method. For each x_i, $i = 0, \ldots, N$, let us denote $\widetilde{C}(x_i, s)$ by $\widetilde{C}(s)$.

We denote the inverse Laplace transform of $\widetilde{C}(s)$ by $\overline{C}(t)$ which is

$$\overline{C}(t) = \frac{1}{2\pi i}\int_{\alpha - i\infty}^{\alpha + i\infty} \mathrm{e}^{st}\widetilde{C}(s)\, ds,$$

and can be expressed as

$$\overline{C}\,(t) = \frac{1}{\pi}\mathrm{e}^{\alpha t}\int_0^\infty \mathrm{Re}\left\{\widetilde{C}\,(s)\,\mathrm{e}^{i\omega t}\right\}d\omega,$$

where $s = \alpha + i\omega$. Using the trapezoidal rule, with step size π/T, we obtain

$$\overline{C}(t) = \frac{1}{T}\mathrm{e}^{\alpha t}\left[\frac{\widetilde{C}\,(\alpha)}{2} + \sum_{k=1}^{\infty}\mathrm{Re}\left\{\widetilde{C}\left(\alpha + \frac{ik\pi}{T}\right)\mathrm{e}^{\frac{ik\pi t}{T}}\right\}\right] - E_T, \tag{22}$$

for $0 < t < 2T$ and where E_T is the discretisation error. It is known that the infinite series in this equation converges very slowly. To accelerate the convergence, we apply the quotient-difference algorithm, proposed in [1], to calculate the series in (22) by the rational approximation in the form of a continued fraction. Under some conditions we can always associate a continued fraction to a given power series.

We denote $v\,(z)$ the continued fraction

$$v\,(z) = d_0/\left(1 + d_1 z/\left(1 + d_2 z/\left(1 + \cdots\right)\right)\right) \tag{23}$$

associated to the power series in (22), that is,

$$v\,(z) = \frac{\widetilde{C}\,(\alpha)}{2} + \sum_{k=1}^{\infty}\widetilde{C}\left(\alpha + \frac{ik\pi}{T}\right)z^k, \tag{24}$$

where

$$z = \mathrm{e}^{i\pi t/T}.$$

Let the M-th partial fraction $v(z, M)$ be

$$v\,(z, M) = d_0/\left(1 + d_1 z/\left(1 + d_2 z/\left(1 + \cdots + d_M z\right)\right)\right).$$

We denote E_F^M the truncation error associated to the continued fraction, that is,

$$v\,(z) = v\,(z, M) + E_F^M.$$

Then

$$\overline{C}\,(t) = \frac{1}{T}\mathrm{e}^{\alpha t}\mathrm{Re}\left\{v\,(z, M) + E_F^M\right\} - E_T.$$

The approximation for $\overline{C}\,(t)$ is denoted by $C(t)$ and given by

$$C\,(t) = \frac{1}{T}\mathrm{e}^{\alpha t}\mathrm{Re}\left\{v\,(z, M)\right\}.$$

3. The discretisation error

To solve the partial differential equation (6) firstly we apply a Laplace transform in t, to obtain the ordinary differential equation in x (11). Equation (11) is then approximated using different spatial discretisations as described in the previous section. Let us denote by $\widetilde{E}_S$ the error associated to the spatial discretisation, that is, $\widetilde{E}_S$ is such that

$$\widetilde{c}(x_i, s) = \widetilde{C}(x_i, s) + \widetilde{E}_S(x_i, s). \tag{25}$$

The next errors come from the numerical inversion of Laplace transform, where the Laplace inverse transform of $\widetilde{C}(x_i, s)$ is, as described in the previous section, the solution

$$\overline{C}\,(x_i, t) = \frac{1}{T}\mathrm{e}^{\alpha t}\mathrm{Re}\left\{v\,(z, M_i) + E_F^M(x_i, t)\right\} - E_T(x_i, t), \tag{26}$$

where E_T is the error associated with the trapezoidal approximation and E_F^M is the truncation error associated to the continued fraction. Note that for each x_i the algorithm chooses an M_i and therefore for each x_i we have a different value of the approximation of the continued fraction, $v\,(z, M_i)$. Therefore from (25)–(26) we have

$$c(x_i, t) = \frac{1}{T}\mathrm{e}^{\alpha t}\mathrm{Re}\left\{v\,(z, M_i) + E_F^M(x_i, t)\right\} - E_T(x_i, t) + E_S(x_i, t),$$

where $E_S(x_i, t)$ is the inverse Laplace transform of the error $\widetilde{E}_S(x_i, s)$.

The error E_T that comes from the integral approximation using the trapezoidal rule, according to Crump [5], is

$$E_T = \sum_{n=1}^{\infty} \mathrm{e}^{-2n\alpha T} c(x_i, 2nT + t).$$

Assume now that our function is bounded such as $|c(x_i, t)| \leq \mathrm{e}^{\sigma t}$, for all x_i. Therefore the error can be bounded by

$$E_T \leq \mathrm{e}^{\sigma t} \sum_{n=1}^{\infty} \mathrm{e}^{-2nT(\alpha-\sigma)} = \frac{\mathrm{e}^{\sigma t}}{\mathrm{e}^{2T(\alpha-\sigma)} - 1}, \quad 0 < t < 2T.$$

It follows that by choosing α sufficiently larger than σ, we can make E_T as small as desired. For practical purposes and in order to choose a convenient α we use the inequality which bounds the error

$$E_T \leq \mathrm{e}^{\sigma t - 2T(\alpha-\sigma)}.$$

If we want to have the bound $E_T \leq b_T$ then by applying the logarithm in both sides of the previous inequality we have

$$\alpha \geq \sigma \frac{2T+t}{2T} - \frac{1}{2T} \ln \left(b_T \right).$$

Assuming $\sigma \geq 0$ we can write

$$\alpha \geq \sigma - \frac{\ln \left(b_T \right)}{2T}.$$

In our example we consider $\sigma = 0$. In practice the trapezoidal error E_T is controlled by the parameter α we choose.

The second error, E_F^M comes from the approximation of the continued fraction given by (24). This error is controlled by imposing a tolerance TOL such as

$$\left| v\left(z, M\right) - v\left(z, M-1\right) \right| < TOL,$$

in order to get the approximation $C\left(x_i, t\right)$ given by

$$C\left(x_i, t\right) = \frac{1}{T} \mathrm{e}^{\alpha t} \mathrm{Re}\{ v\left(z, M_i\right) \},$$

where M_i changes according to which x_i we are considering.

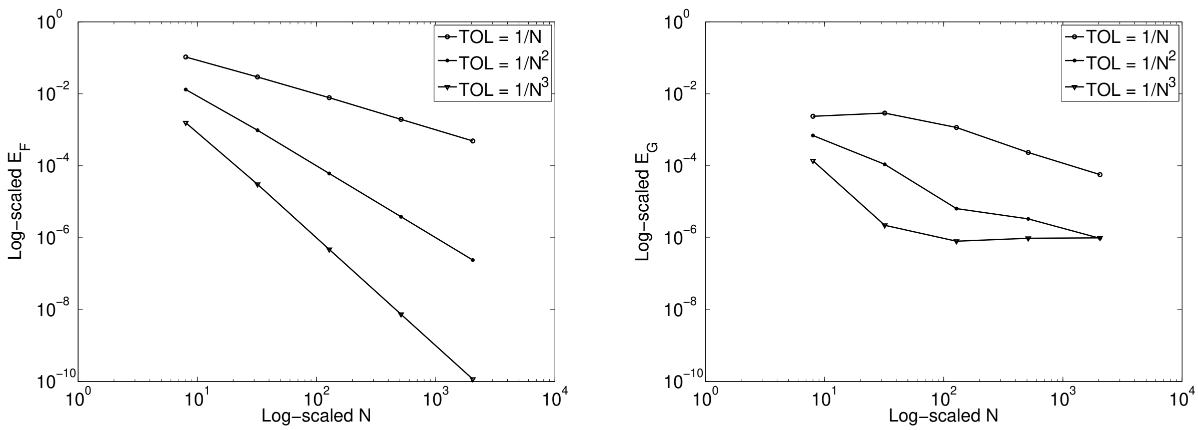

FIGURE 1. Error E_F and E_G for $\theta = 0$, $P = 2$, $t = 1$, $0 \leq x \leq 10$ and $\alpha = 10^{-6}$ and different values of TOL. The global error is controlled by the parameter α.

In order to understand better how we control the trapezoidal error with the parameter α and how the tolerance TOL affects the error we present a practical example. We assume P constant, in order to not consider a spatial

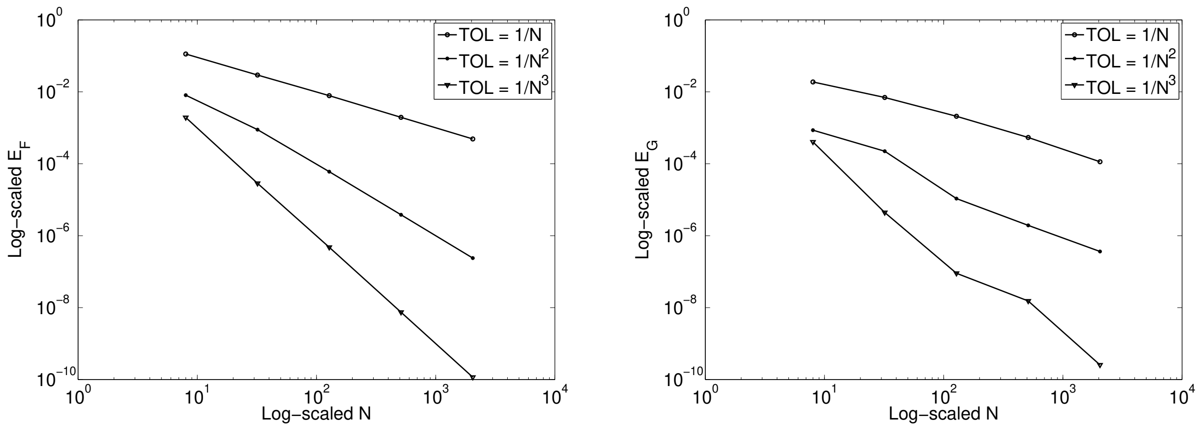

FIGURE 2. Error E_F and E_G for $\theta = 0$, $P = 2$, $t = 1$, $0 \leq x \leq 10$ and $\alpha = 10^{-10}$ and different values of TOL. The parameter α is chosen such that the global error is not affected.

discretisation, since when P is constant we can apply directly the inverse Laplace transform to the exact solution (14).

For $\theta = 0$, P constant and $c\,(0, t) = c_0$, the analytical solution is

$$c\,(x, t) = \frac{c_0}{2}\left(\mathrm{erfc}\left[\frac{x + Pt}{2\sqrt{Dt}}\right] + \mathrm{e}^{-Px/D}\mathrm{erfc}\left[\frac{x - Pt}{2\sqrt{Dt}}\right]\right).$$

In Figures 1 and 2, for $P = 2$, $t = 1$ and $0 \leq x \leq 10$, we plot the following errors,

$$E_F = \max_{1 \leq i \leq N-1} |v(z, M_i) - v(z, M_i - 1)| \quad \text{and} \quad E_G = ||c(x_i, t) - C(x_i, t)||_\infty,$$

where $|| \cdot ||_\infty$ is the infinity norm. The error E_F is related with the error E_F^M since we control E_F^M by controlling E_F with the tolerance TOL. Figures 1 and 2 show how the parameter α, given by $\alpha = -\ln(10^{-6})/2T$ in Figure 1 and $\alpha = -\ln(10^{-10})/2T$ in Figure 2, affect the global convergence. Note that in Figure 1 the precision does not go further than 10^{-6}. The global error of Figure 1 and Figure 2 is not affected by the spatial error E_S since we apply the Laplace inversion algorithm directly in (14).

The Laplace inversion algorithm approximates the value of the infinite series using a truncated continued fraction and this truncation is done by choosing an M_i for each x_i. This M_i is chosen according to which value of the tolerance TOL we consider. We show in Figure 3 the variations of M_i and it is clear the algorithm concentrates the high values of M in the region that presents steep gradients.

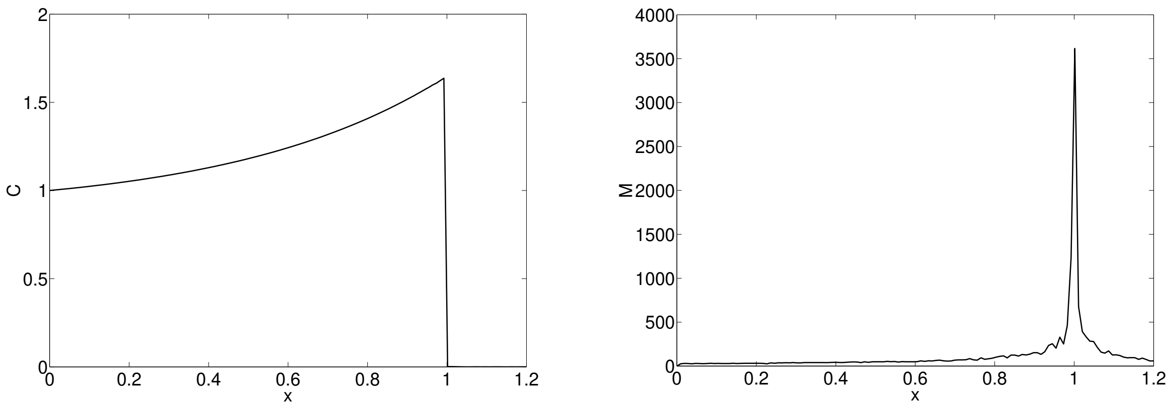

FIGURE 3. Number of iterations M for $\theta = 1$, $P = -2$, $t = 1$ and $TOL = 1/N^2$.The figure on the left represents the approximated solution. The figure on the right is the number of M iterations we need to run for each x_i.

To finish this section we add some few comments about the error E_F^M. In practice it is very difficult to choose an M according to a theoretical result since the analytical errors we can get for continued fractions are strongly dependent on the d_k's. Additionally, to prove the analytical convergence of the algorithm is not an easy task. The following theorem [12], although restrictive in what concern the variables d_k, it can be applied in some of our examples.

Theorem 3.1. *Let $\{Q_M\}$ be a sequence of complex numbers $Q_M = q_M \mathrm{e}^{i\psi_M}$ such that*

$$\left| Q_M - \frac{1}{2} \right| \le \frac{1}{2} - \varepsilon, \qquad 0 < \varepsilon < \frac{1}{2}, \qquad M = 0, 1, 2, \ldots.$$

Let $\{E_M\}$ be the sequence of parabolic regions defined by

$$E_M = \left\{ \omega : |\omega| - \mathrm{Re}\left(\omega \mathrm{e}^{-i(\psi_M + \psi_{M-1})} \right) \le 2kq_{M-1} \left(\cos\psi_M - q_M \right) \right\}, \qquad (27)$$

where $0 < k < 1$. If $v(z)$ is a continued fraction (23) with elements satisfying

$$d_0 \in E_1, d_M z \in E_{M+1},\ M = 1, 2, \ldots, \qquad 0 < |d_M z| < L,\ M = 0, 1, 2, \ldots,$$

for some $L > 0$, then $v(z)$ converges to a finite value v and

$$|v - v(z, M)| \le \frac{|d_0| \left(\cos\psi_1 - q_1 \right)}{\left(1 + \varepsilon^2 \frac{(1-k)}{L} \right)^{M-1}}, \qquad M = 2, 3, 4, \ldots.$$

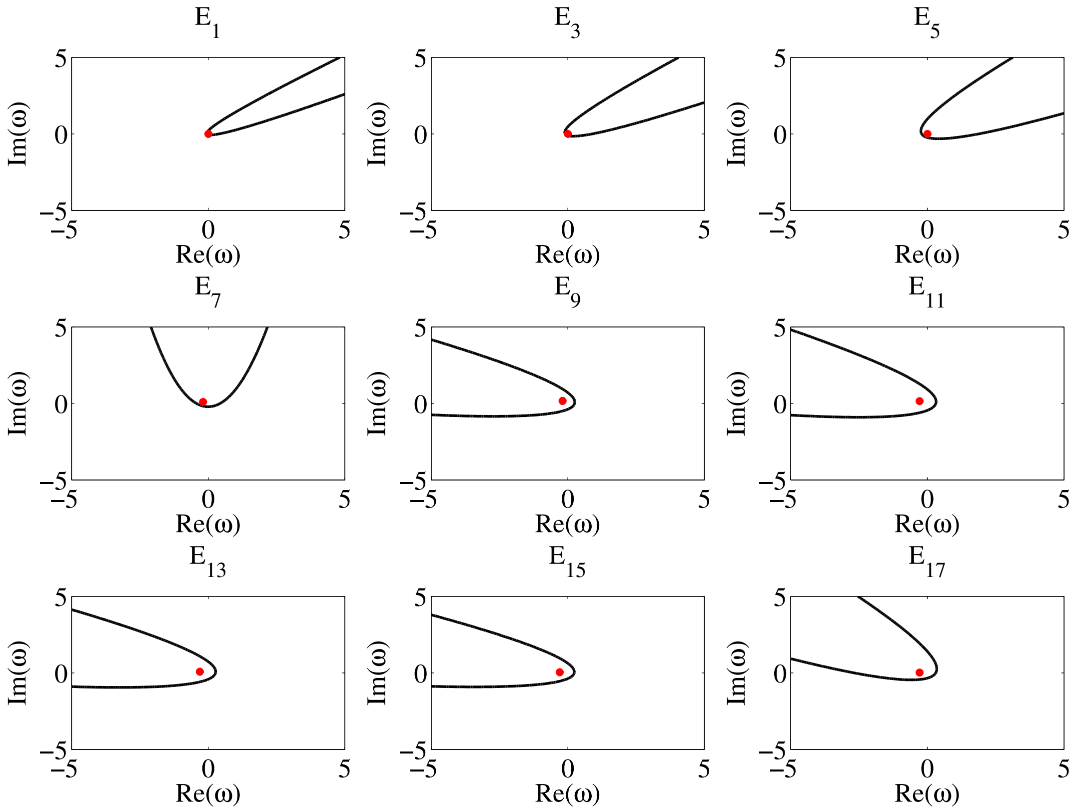

FIGURE 4. The regions are defined by E_M given in (27). The parameters $d_k \in E_{k+1}$ are represented by the points inside the parabolas.

We show an application of Theorem 3.1, since it is illustrative of the complexity of the theoretical results. The example considers $\theta = 0$, $P = 0$, $t = 1$ and $TOL = \frac{1}{N}$. By running the inverse Laplace algorithm, we obtain the d_k values that define the truncated continued fraction $v(z, M)$. In Figure 4 we plot some of the parameters d_k and show the d_k's are inside parabolic regions defined by E_M in (27).

4. Numerical Tests

In this section we analyse different aspects of the space discretisations described in section 2. In all of our examples we consider $D = 1$. In the end we show the solution for different values of t, P and θ in order to understand the physical role of these parameters.

4.1. Convergence of the space discretisations. In this section we start to display some figures that show how the different space discretisations deal with different values of θ and P. Since we do not have an exact solution for $\theta \neq 0$ we compare the approximated solution with the solution $\overline{c}(x,t)$ obtained from applying the numerical inverse Laplace transform algorithm to the solution (14), for $c_0 = 1$, which is given by

$$\widetilde{c}\,(x,s) = \frac{1}{s}\mathrm{e}^{\nu_s^- x}.$$

The solution $\overline{c}(x,t)$ is not affected by the spatial error and therefore when compared with the approximated solution C gives an indication of the numerical problems that are associated with the spatial discretisation.

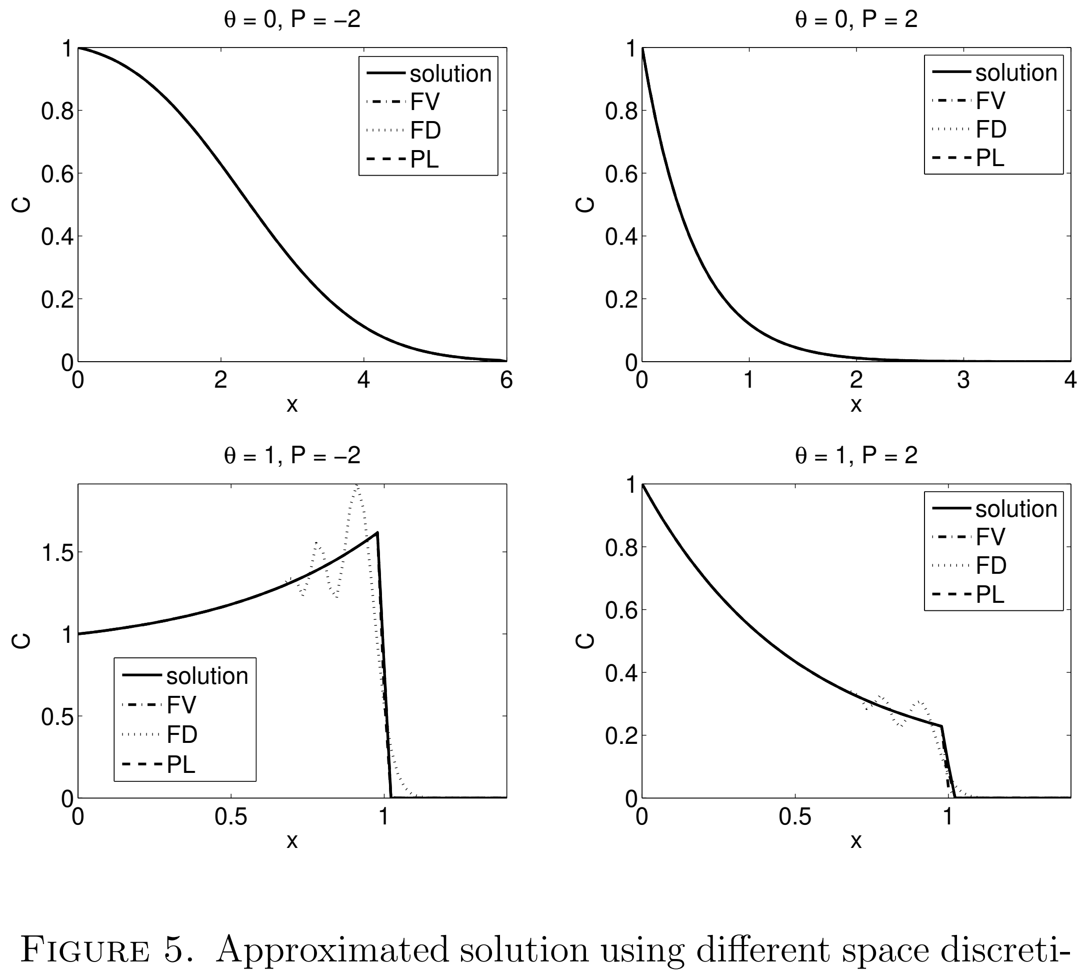

FIGURE 5. Approximated solution using different space discretisations, for different values of P and θ at $t = 1$ for $N = 64$. The $-$ solution refers to the solution $\overline{c}(x,t)$.

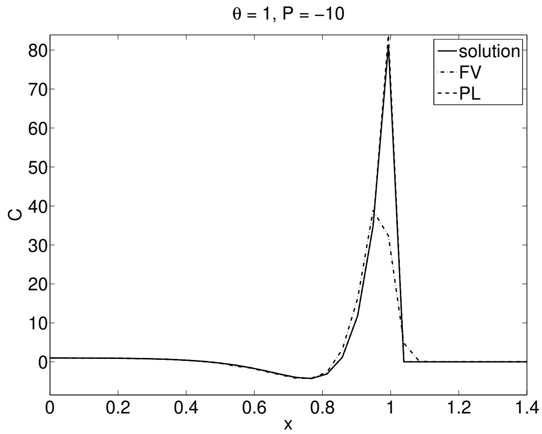

FIGURE 6. Approximated solution using finite volumes method and the piecewise linearized method. The $-$ solution refers to the solution $\overline{c}(x,t)$.

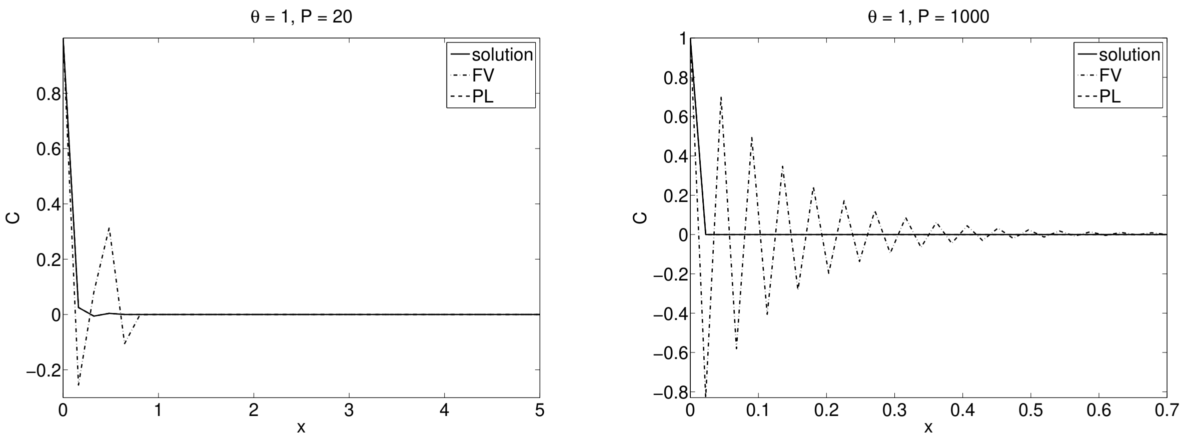

FIGURE 7. Approximated solution using the finite volumes and the piecewise approximation for $N = 32$. The finite volumes method shows more oscillations. The $-$ solution refers to the solution $\overline{c}(x,t)$.

In Figure 5, we consider a parabolic case, for $\theta = 0$, and a hyperbolic case for $\theta = 1$. The finite volume formulation (FV), the piecewise linearized method (PL) and the finite difference schemes (FD) are compared. The finite volume formulation has a similar behavior to the piecewise linearized method although for the case $\theta = 1$, $P = 2$ we can see a slightly better behavior for the piecewise linearized method. The finite differences method performs worst than the other two methods since oscillations are not avoided for small space steps.

In Figure 6 we display another example comparing the finite volumes method with the piecewise linearized method and this performs better than the finite volume method. In Figure 6 the piecewise linearized method coincides with the line of the solution we are using to test the performance of the methods and therefore it is not visible.

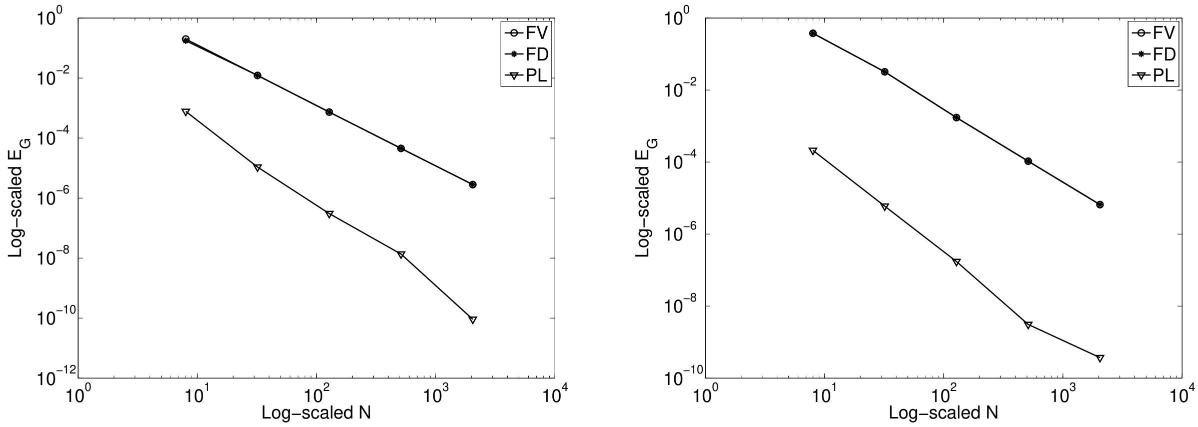

FIGURE 8. Rate of convergence for the space discretisations where $\theta = 0$, $t = 1$, $TOL = 1/N^3$, $\alpha = 10^{-16}$: (a) $P = 2$, $t = 1$ and $0 \leq x \leq 10$; (b) $P = 10$, $t = 1$, $0 \leq x \leq 3$.

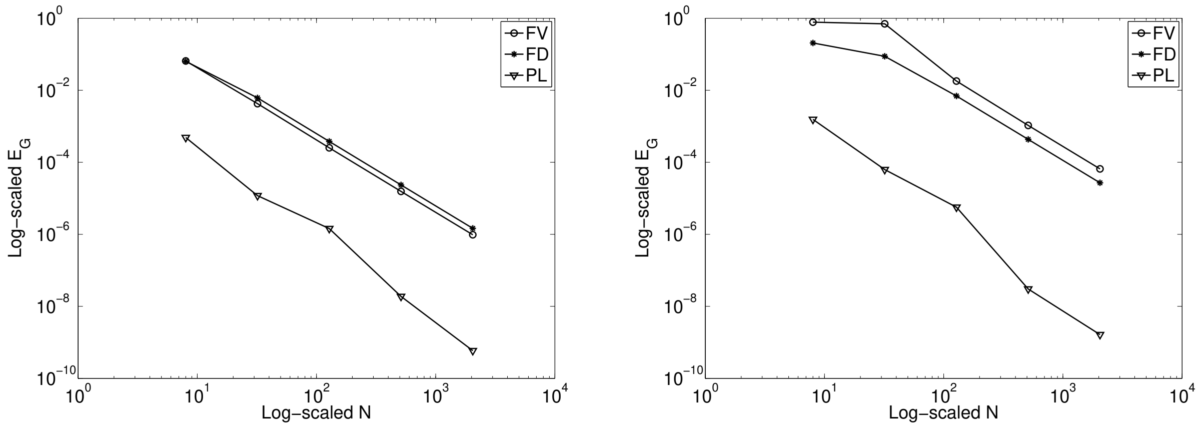

FIGURE 9. Rate of convergence for the space discretisations where $\theta = 0$, $t = 1$, $TOL = 1/N^3$, $\alpha = 10^{-16}$: (a) $P = -2$, $t = 1$ and $0 \leq x \leq 12$; (b) $P = -10$, $t = 1$, $0 \leq x \leq 22$.

Additionally the finite volume method in certain situations oscillates as shown in Figure 7. In Figure 7 we show two examples for $\theta = 1$ with $P = 20$ and $P = 1000$. For $P = 20$ we have a large space step and for $P = 1000$

we have a small space step. Therefore for small space steps and large P oscillations are not avoided.

To have information about the space discretisation errors we show the global error in Figures 8 and 9 for the three schemes. We consider $\theta = 0$ and P constant since it is the example we have access to an exact solution. We observe the piecewise linearized method has a smaller error than the other two schemes. In Figure 8 for $P = 2$ and $P = 10$ the rate of convergence for the finite volumes and finite differences methods is around 2.0. The rate of convergence for the piecewise linearized method is 2.9 for $P = 2$ and is 2.3 for $P = 10$. Therefore, it has a significant higher order than the other two schemes. In Figure 9 for $P = -2$ the finite volume and finite difference methods have a rate of convergence of order around 2.0 and for $P = -10$ is around 1.7. The piecewise linearized scheme in both situations has a rate of convergence around 2.5. We can conclude that in general the piecewise linearized method is a better choice.

In the next section we display some figures that help us to understand the behavior of the exact solution of the differential equation (6) according to which values of θ and P we choose.

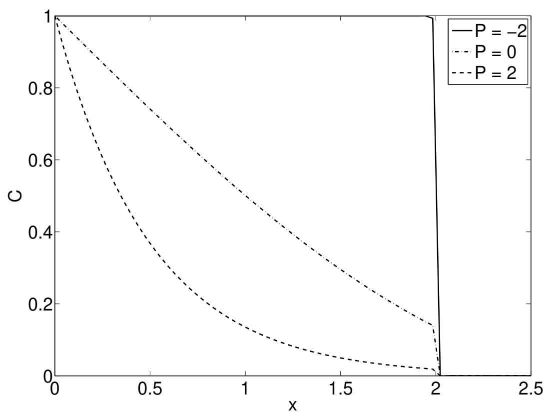

FIGURE 10. Solution for time $t = 1$.

4.2. Behavior of the solution. The solutions in this section are obtained by running the algorithm with the piecewise linearized method. First we consider the problem with boundary condition $c(0,t) = 1$ and P constant, that is, we consider the partial differential equation,

$$\frac{\partial c}{\partial t} + \theta \frac{\partial^2 c}{\partial t^2} = P \frac{\partial c}{\partial x} + D \frac{\partial^2 c}{\partial x^2}. \tag{28}$$

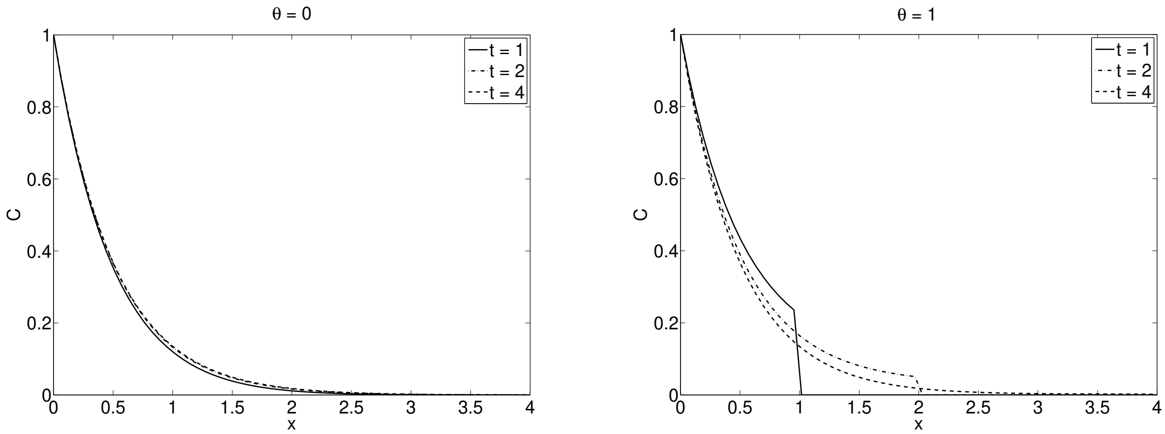

FIGURE 11. Behavior of the solution as we travel in time for $P = -2$.

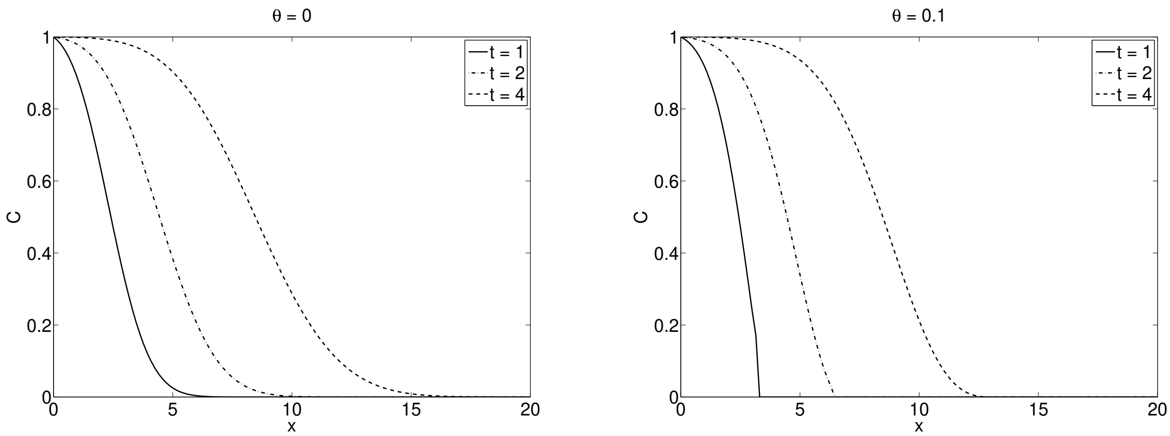

FIGURE 12. Behavior of the solution as we travel in time for $P = 2$.

We have a discontinuous initial solution at $x = 0$ and since the equation is hyperbolic for $\theta \neq 0$ the discontinuity is transported along the characteristics. The characteristic equation associated to equation (28) is

$$\theta \left(\frac{dx}{dt}\right)^2 - D = 0.$$

The characteristic curves are given by $x = t\sqrt{\frac{D}{\theta}} + \xi$ and the waves are transmitted with velocity $v = \sqrt{D/\theta}$. At $\xi = 0$ we have $x = t\sqrt{\frac{D}{\theta}}$. For $\theta = 1/4$ and $D = 1$, the discontinuity at $t = 1$ appears at $x = 2$ as shown in Figure 10. We also notice that the discontinuity does not depend on the value of P.

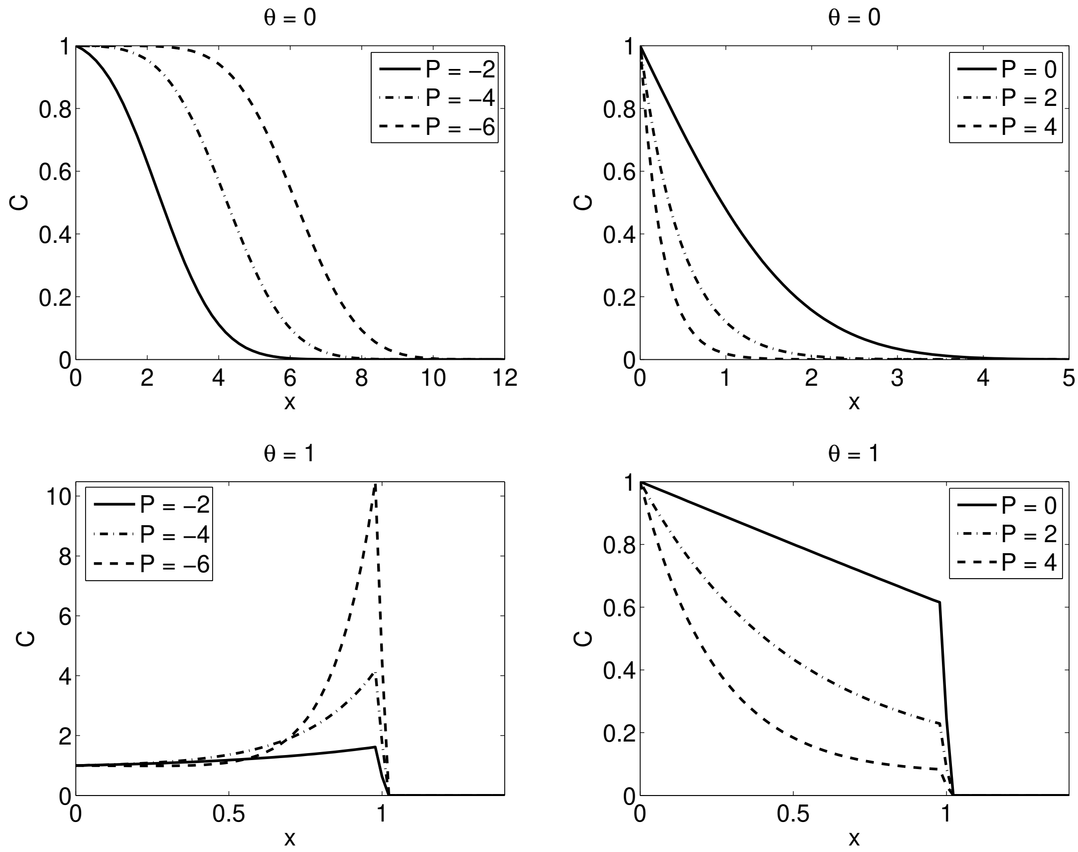

FIGURE 13. The influence of P in the solution.

In Figure 11 and 12 we display the behavior of the mass concentration C as we travel in time. In Figure 11, the jump discontinuity quickly dissipates with time. This means that the non-Fickian effects are more significative in short times. As t increases, the hyperbolic solution tends to the parabolic solution.

Figure 13 shows the effect of the parameter P in the solution. The peak increases with $|P|$ for $P < 0$ and decreases with $|P|$ for $P > 0$. The jump discontinuity at a specific time is the same for different values of P. This phenomena is explained from the definition of the propagation speed, which do not depend on P.

Figure 14 shows the behavior of the solution as we change the parameter θ. When θ increases, the hyperbolic effects start to appear in a lower point x, that is, the velocity decreases with θ as the jump discontinuity peak increases.

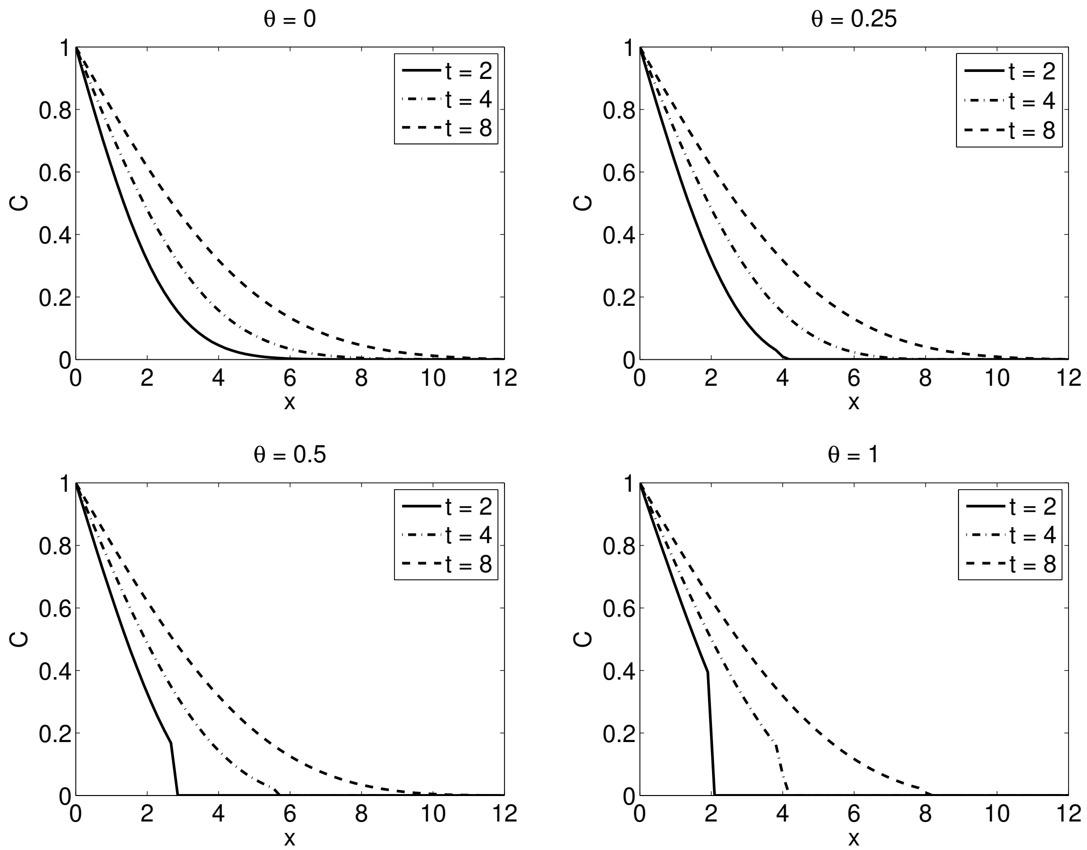

FIGURE 14. Behavior of the solution as we change θ, for $P = 0$.

Let us now consider the case where the potential P is non-constant. Observing the profile of C for various time instants from Figures 15 and 16, we can deduce that the hyperbolic differential equation is sensitive to changes in the potential field. In Figure 15, for $P(x) = -2x$ and $P(x) = 2x$, we observe the solutions have different profiles. In Figure 16 we consider $P(x) = -2\mathrm{e}^{-x}$ and $P(x) = 2\mathrm{e}^{-x}$. This figure when compared with Figure 15 can lead us to conclude that the profile of the solution seems to be quite different between negative potential fields whereas for positive potential fields seems to be more similar.

In Figures 17 and 18 we consider $P(x) = Px$ and $P(x) = P\mathrm{e}^{-x}$ respectively, for different values of P. It is shown that the influence of the potential field is quite significant. As stated before, we observe in these figures that, the location of the jump discontinuity does not depend on P. Furthermore, the position of the mass wave front is still $t\sqrt{\frac{D}{\theta}}$.

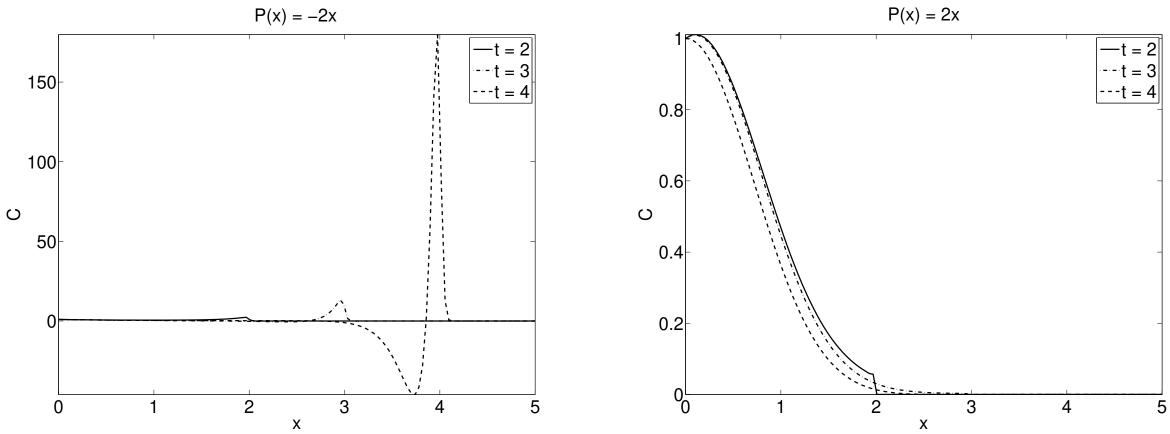

FIGURE 15. Solutions for a non-constant potential and $\theta = 1$.

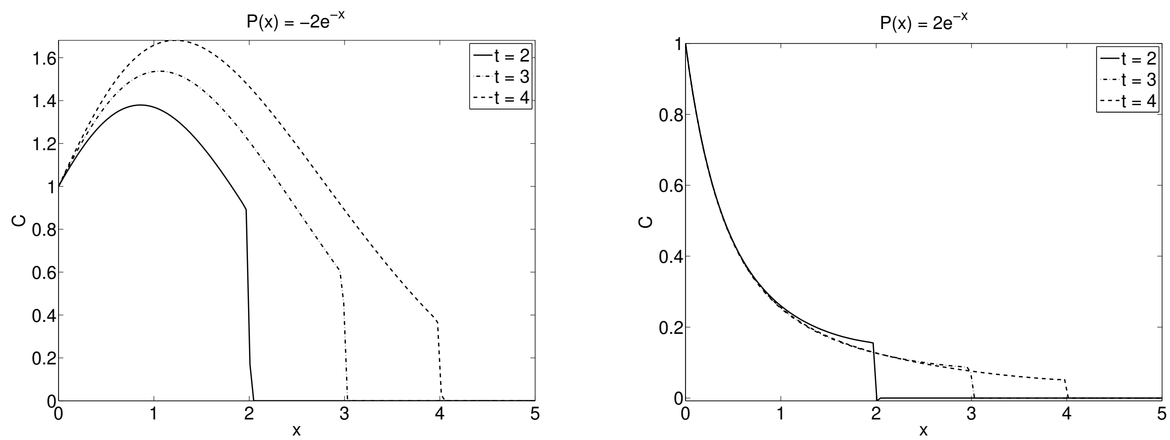

FIGURE 16. Solutions for a non-constant potential and $\theta = 1$.

Another solution is considered by assuming $c(0,t) = \mathrm{e}^{-t}$ at the inflow boundary (9). In this case, equation (14) changes to

$$\widetilde{C}\,(x,s) = \frac{1}{s+1}\mathrm{e}^{\nu_s^- x}.$$

Comparing Figures 19 and 20 with Figure 13 we observe that the change of the boundary condition does not produce a very strong effect in the way the mass concentration C behaves, that is, the profile of the solutions have similarities. Note that for this case we also have a discontinuity at $x = 0$.

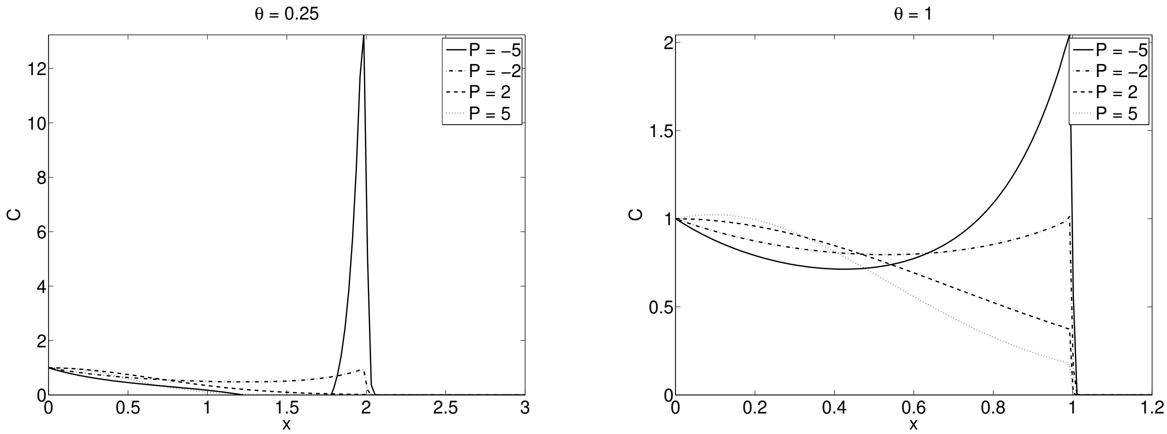

FIGURE 17. Solutions for a non-constant potential $P(x) = Px$.

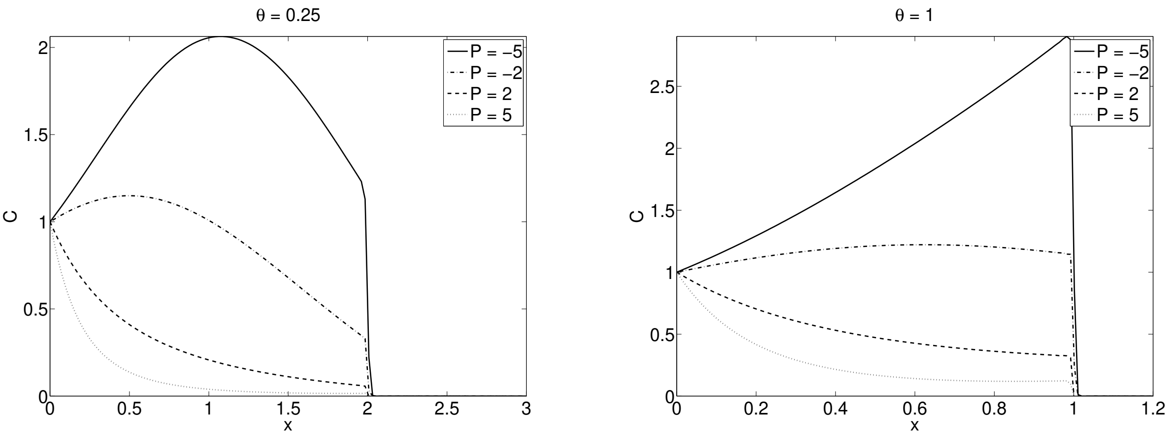

FIGURE 18. Solutions for a non-constant potential $P(x) = P\mathrm{e}^{-x}$.

We have seen that the solution is affected by the values of θ and P we consider. For θ very close to zero, we have a parabolic equation and therefore the solution is smooth for different values of P. For $\theta \neq 0$ and close to one we have a hyperbolic equation which transports the initial discontinuity at the inflow boundary. Such discontinuity dissipates as we travel in time.

References

[1] Ahn J, Kang S, Kwon Y, A flexible inverse Laplace transform algorithm and its application, *Computing* **71(2)**: 115-131, 2003.

[2] Chen H-T, Liu K-C, Numerical analysis of non-Fickian diffusion problems in a potential field, *Numerical Heat Transfer*, **Part B, 40**: 265-282, 2001.

[3] Chen H-T, Liu, K-C, Analysis of non-Fickian diffusion problems in a composite medium, *Computer Physics Communications* **150**: 31-42, 2003.

[4] Crank J, *The Mathematics of Diffusion*, Oxford University Press, 1974.

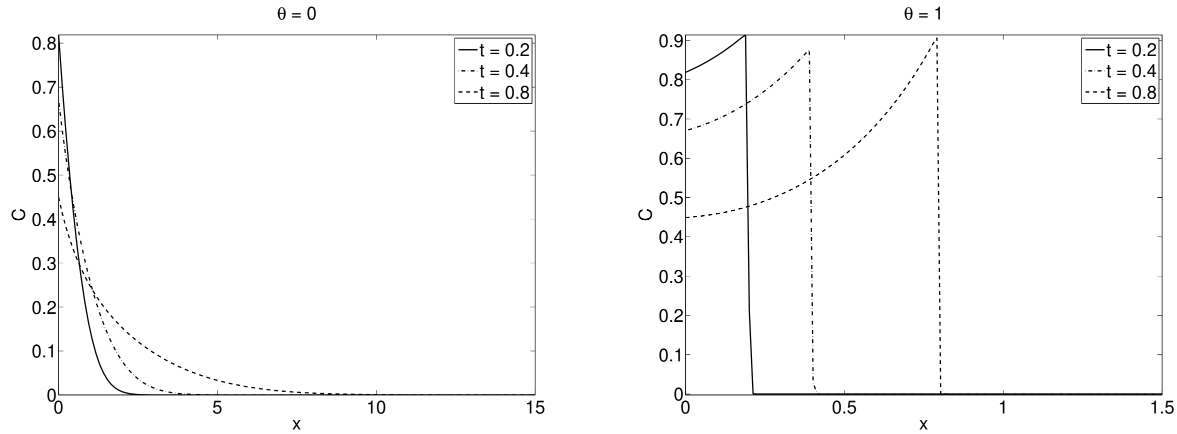

FIGURE 19. Solutions for time dependent boundary condition $c(0,t) = \mathrm{e}^{-t}$ and $P(x) = -2x$

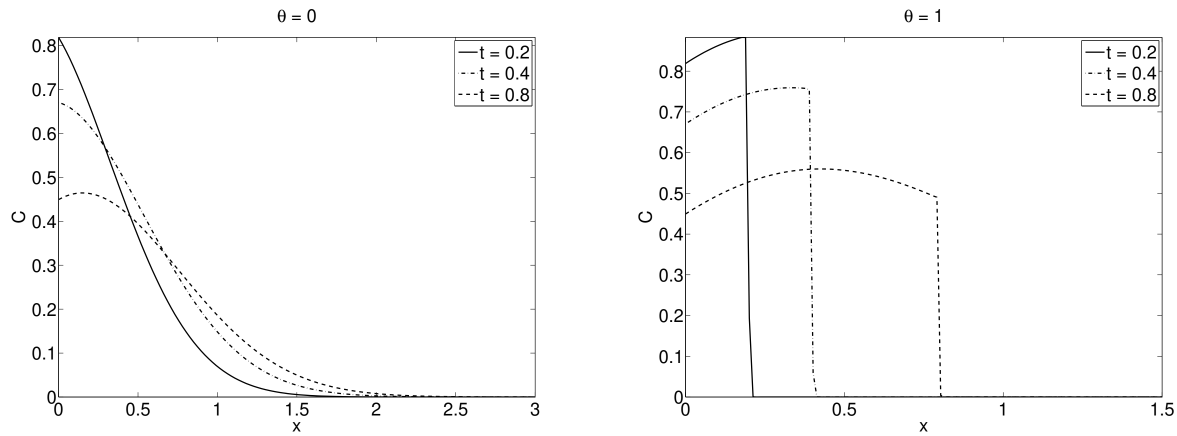

FIGURE 20. Solutions for time dependent boundary condition $c(0,t) = \mathrm{e}^{-t}$ and $P(x) = 2x$.

[5] Crump K, Numerical inversion of Laplace transforms using a Fourier series approximation, *Journal of the Association for Computing Machinery* **23(1)**: 89-96, 1976.
[6] Das AK, A non-Fickian diffusion equation, *J. Appl. Phys* **70**: 1355-1358, 1991.
[7] Das AK, Some non-Fickian diffusion equations: Theory and Applications, *Defect and Diffusion Forum* **162-163**: 97-118, 1998.
[8] Fedotov S, Traveling waves in a reactiondiffusion system: diffusion with finite velocity and Kolmogorov-Petrovskii-Piskunov kinetics, *Physical Review E* **4**: 51435145, 1998. 51435145.
[9] Hassanizadeh SM, On the transient non-Fickian dispersion theory, *Transport in Porous Media*, **23**: 107-124, 1996.
[10] Joseph DD, Preziosi L, Heat waves, *Reviews of Modern Physics*, **61**: 4173, 1989.
[11] Kubo R, Toda M, Hashitsume N, *Statistical Physics II*, Springer Series in Solid-State Sciences, 31, Springer, 1978.
[12] Jones W, Thron W, *Continued Fractions: Analytic Theory and Applications*, Encyclopedia of Mathematics and its Applications, 11, 1980.

[13] Liu K-C, Chen H-T, Numerical analysis for the hyperbolic heat conduction problem under a pulsed surface disturbance, *Applied Mathematics and Computation* **159**: 887-901, 2004.
[14] Ramos JI, On the numerical treatment of an ordinary differential equation arising in one-dimensional non-Fickian diffusion problems, *Computer Physics Communications* **170**: 231-238, 2005.
[15] Strack ODL, A mathematical model for dispersion with a moving front in groundwater, *Water Resour. Res.*, **28(11)**: 2973-2980, 1992.

A. Araújo
CMUC, Department of Mathematics, University of Coimbra, 3001-454 Coimbra, Portugal
E-mail address: alma@mat.uc.pt

C. Neves
ISCAC, Instituto Politécnico de Coimbra, 3040-316 Coimbra, Portugal and Department of Mathematics, University of Coimbra, 3001-454 Coimbra, Portugal
E-mail address: cneves@iscac.pt

E. Sousa
CMUC, Department of Mathematics, University of Coimbra, 3001-454 Coimbra, Portugal
E-mail address: ecs@mat.uc.pt